Superlattices and Microstructures 33 (2003) 217–226

Superlattices and Microstructures

www.elsevier.com/locate/jnlabr/yspmi

Electrical characterization of metal–molecule–silicon junctions

W. Wang[a], T. Lee[a], M. Kamdar[a], M.A. Reed[a,*], M.P. Stewart[b], J.-J. Hwang[b], J.M. Tour[b,*]

[a] *Departments of Electrical Engineering, Applied Physics, and Physics, Yale University, P.O. Box 208284, New Haven, CT 06520, USA*

[b] *Department of Chemistry and Center for Nanoscale Science and Technology, Rice University, MS 222, 6100 Main Street, Houston, TX 77005, USA*

Received 20 February 2003; received in revised form 22 August 2003; accepted 1 September 2003

Abstract

Direct assembly of molecules onto silicon surfaces is of particular interest for potential employment in hybrid organic-semiconductor devices. In this study, aryl diazonium salts are used to assemble covalently bound molecular groups onto a hydride-passivated, oxide-free n-type Si(111) surface. The reaction of 4-(trimethylsilylethynyl)benzenediazonium tetrafluoroborate generates a molecular layer of 4-(trimethylsilylethynyl)phenylene (TMS-EP) on the Si surface. The monolayer modifies the electrical properties of the interface and exhibits nonlinear current–voltage characteristics, as compared with the ohmic behavior observed from metal-n^{++}-Si(111) junctions. Results of current–voltage measurements at variable temperatures (from 300 to 10 K) on samples made with the TMS-EP molecules do not show significant thermally-activated transport, indicating tunneling is the dominant transport mechanism for this device structure. The measured data is compared to a tunneling model.
© 2003 Elsevier Ltd. All rights reserved.

Keywords: Hybrid organic-semiconductor devices; Silicon; Diazonium; Tunneling

1. Introduction

The ability to utilize single molecules as electronic devices has motivated researchers for years in the pursuit of miniaturizing electronic circuit elements [1]. To study the

* Corresponding authors.
E-mail addresses: mark.reed@yale.edu (M.A. Reed), tour@rice.edu (J.M. Tour).

0749-6036/$ - see front matter © 2003 Elsevier Ltd. All rights reserved.
doi:10.1016/S0749-6036(03)00081-8

electronic transport through molecular layers, a commonly used method is to form metal/molecule/metal junctions [2–6]. Another interesting research direction of recent years is to combine functional organic molecules with semiconductors [7, 8]. Several groups have studied electronic transport properties for molecule/semiconductor junctions using Si [9–11], GaAs [12], and organic semiconducting materials [13] as the substrates. The molecule/semiconductor system is of particular interest for the potential control of electronic properties at the interface. For example, it has been reported that molecules can modify (in a controllable way) the Schottky barrier in metal/molecule/GaAs systems [12] and metal/molecule/organic semiconductor junctions [13] due to the dipole moment formed at the interface.

Electrochemical grafting of aryl groups onto carbon [14] and silicon [15] electrode surfaces from diazonium salt precursors has been shown previously via heterogeneous phase reduction [16]. Aryl diazonium salts [17] can be used alone, in the absence of an externally applied potential, to assemble covalently bound conjugated monolayers on the Si(111):H surface [18]. This type of organic monolayer on Si has demonstrated exceptionally high electrochemical passivation and chemical endurance [18, 19]. In our study, 4-(trimethylsilylethynyl)benzenediazonium tetrafluoroborate is used to form the organic layer of 4-(trimethylsilylethynyl)phenylene (TMS-EP) on the Si surface. TMS-EP was chosen because it is a simple diazonium salt that has been experimentally determined to give reproducible layer thickness. Electrical characterizations such as temperature-dependent current voltage ($I(V, T)$) measurements are performed to investigate the charge transport mechanisms through such a TMS-EP layer.

2. Experimental

Electronic transport measurements on molecule/silicon junctions were performed using microfabricated devices. A schematic diagram of such a device is illustrated in Fig. 1. The device fabrication starts with highly doped (arsenic as dopant; resistivity $\rho = 0.001$–$0.005\ \Omega$ cm) n-type Si(111) wafer. After 300 nm SiO_2 is thermally grown on the Si substrate, windows of various sizes (3 μm $\times$ 3 μm to 200 μm $\times$ 200 μm) are opened by standard photolithography and subsequent HF etching. The TMS-EP molecular layer (the schematic of TMS-EP is shown in Fig. 1(b)) is assembled and covalently bound onto a hydride-passivated Si surface that was made by treating the samples with NH_4F for 15 min, as illustrated in Fig. 2. The hydride-terminated Si surface is exposed to a solution of the diazonium salt in anhydrous acetonitrile for a few hours under an inert atmosphere (a nitrogen filled glove box with sub-1 ppm H_2O and O_2) in the dark (Fig. 2(a)). The diazonium salts are believed to be activated by a redox reaction at the open circuit potential of the substrate material in solution, which leads to the local generation of aryl radicals by loss of N_2 and ultimately the formation of irreversible surface-molecule bonds (Fig. 2(b)) [18].

To study the quality of the molecular layer, TMS-EP layers on large pieces of Si wafers were analyzed with a single wavelength ellipsometer and a PHI 5700 X-ray photoelectron spectroscopy (XPS) instrument. Table 1 shows the results of layer thickness measurements, indicating that partial multilayer character could be present in the film.

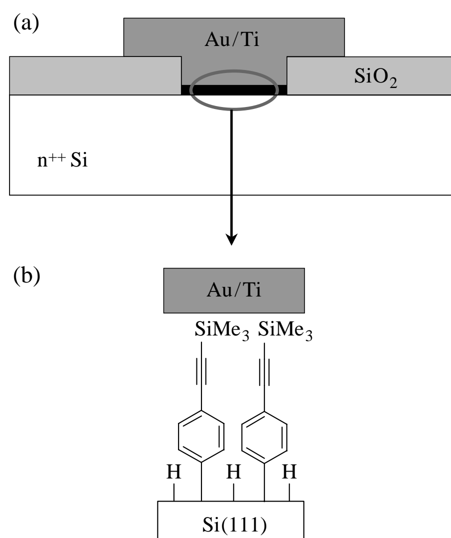

Fig. 1. (a) Schematics of device configuration: n^{++} Si(111) is used as substrate. (b) Schematic showing a molecular junction formed in the device area (circled in (a)). The structure of molecule (TMS-EP) is also shown.

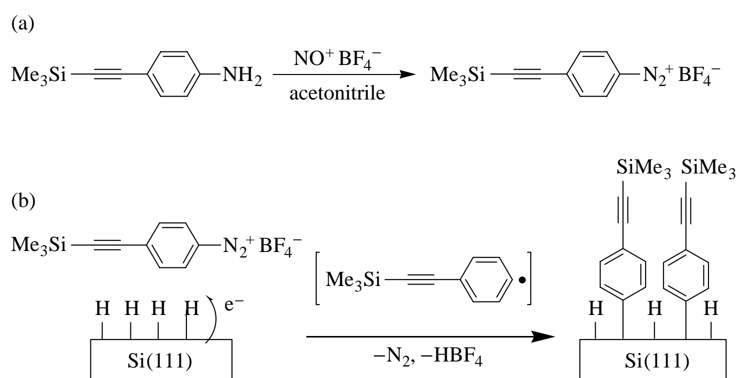

Fig. 2. (a) Synthesis of 4-(trimethylsilylethynyl)benzenediazonium tetrafluoroborate from 4-(trimethylsilylethynyl)aniline and nitrosonium tetrafluoroborate. (b) Reaction of 4-(trimethylsilylethynyl)benzenediazonium tetrafluoroborate with the Si(111):H surface to generate the TMS-EP monolayer.

Table 1
Surface thickness measurement results for the TMS-EP film

Method	Thickness (Å)
Calculation (includes 1.85 Å Si–C bond)	12 ± 1
Single wavelength ellipsometry	16 ± 3
XPS	18 ± 4

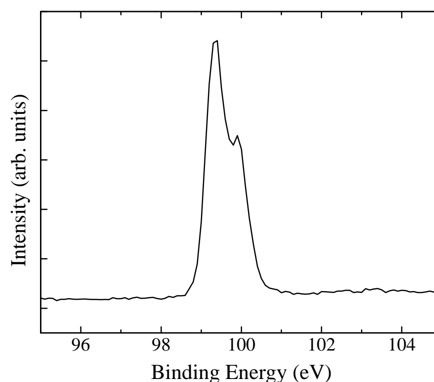

Fig. 3. XPS data showing the Si 2p region of a TMS-EP monolayer sample. The main Si peak is at 99.5 eV and the doublet structure is due to $2p^{1/2}$–$2p^{3/2}$ spin–orbit coupling. The sample is free of the intense SiO_2 signal that would appear at 103 eV.

Ellipsometric measurements of molecular layer thicknesses were taken with a single angle, single wavelength (632.8 nm laser) Gaertner Stokes Ellipsometer. XPS spectra used a monochromated Al Kα source at 350 W and were collected at a 45° takeoff angle, giving a sampling depth of approximately 2 nm (inelastic mean free path). XPS spectral values were referenced to the Si 2p value for a freshly H-terminated Si wafer and the C 1s value for adventitious hydrocarbon residue. Fig. 3 is the XPS data showing the Si 2p region of a TMS-EP-bonded sample made from a large piece of Si wafer. The main Si peak is at 99.5 eV and the doublet structure is due to $2p^{1/2}$–$2p^{3/2}$ spin–orbit coupling. As shown in this figure, the sample is free of the intense SiO_2 signal that would appear at 103 eV [20], which indicates that the molecule/Si interface is free of silicon oxide.

The samples are then transferred under ambient conditions to a thermal evaporator to deposit the top electrode. Five nm Ti followed by 80 nm Au are deposited under a pressure of $\sim 10^{-8}$ Torr at room temperature. The most challenging step in fabricating molecular junctions (vertical structure similar to Fig. 1) is to make the top electrical contact. During the fabrication of metal–SAM–metal junctions, metallic materials deposited on the top of molecules often either penetrate through the thin molecular layer or contact directly with the substrate via defect sites (such as grain boundaries) in the monolayer, causing shorted circuit problems [21, 22]. A low-temperature evaporation technique is often used for the top-side metallization in metal–SAM–metal junction fabrications to avoid the thermal damage to the molecular layer by flowing liquid nitrogen through a cooling stage during the evaporation [2, 23]. In our study on diazonium/Si devices, we have utilized both low temperature and room temperature evaporations and we observed device yield[1] of $\sim$6% (3 working devices out of a total 53 fabricated devices) and $\sim$32% (30 working devices out of a total 94 fabricated devices) for low and room

[1] We define a working device as a sample that is neither open (current < 1 pA at 1 V) nor short (current > 10 mA at 0.5 V), and shows nonlinear $I(V)$ characteristics.

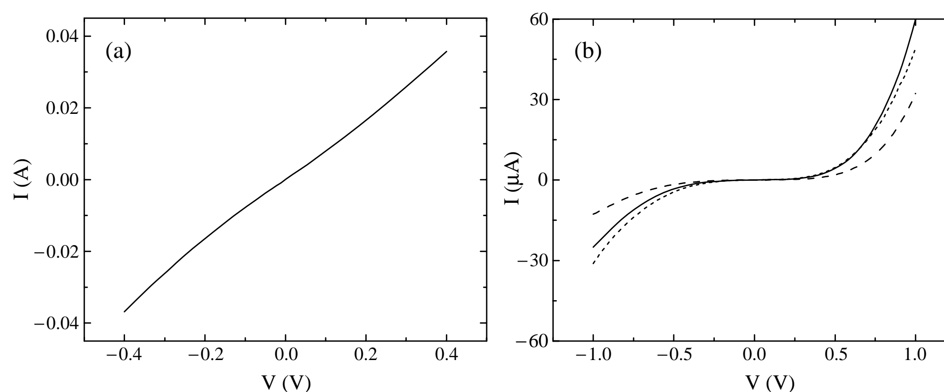

Fig. 4. (a) Typical $I(V)$ of the control device showing ohmic behavior with a resistance of 10 Ω. (b) Representative $I(V)$ data for three metal/TMS-EP/Si junction devices.

temperature evaporations, respectively. In this study we focus on devices fabricated via room temperature metallization. The fabricated devices are measured on a probe station and subsequently packaged for $I(V, T)$ measurements in a Janis cryostat. Two-terminal DC $I(V)$ measurements are performed using a HP4145B semiconductor parameter analyzer.

3. Results

3.1. Current–voltage ($I(V)$) characteristics

Fig. 4(a) is a typical $I(V)$ characteristic of control samples without molecules, which exhibits nearly ohmic behavior with a resistance of 10 Ω (specific contact resistance of $\sim 10^{-6}$ Ω cm^2) due to the highly doped silicon used as the substrate in this study. All of the metal/TMS-EP/Si junction devices showed nonlinear $I(V)$ characteristics with significantly suppressed current densities. Representative $I(V)$ data (measured at room temperature) for three molecular devices are shown in Fig. 4(b). In this figure positive bias corresponds to electron injection from the bottom chemisorbed molecule–silicon contact. Current densities for molecular junctions ($J \sim 5$–10 A cm^{-2} at 1 V; devices for Fig. 4(b)) are reduced roughly by five orders of magnitude as compared with that for the control sample ($J \sim 10^5$ A cm^{-2} at 0.4 V; corresponding to 2.5×10^5 A cm^{-2} at 1 V; device for Fig. 4(a)) due to the molecular layer acting as an insulating barrier.

We observed device-to-device variations of current densities and $I(V)$ shapes. Fig. 5 shows a histogram plot for observed current densities (at 1 V) of all the working molecular devices[2]. Note that J (x-axis) is on a log scale in this plot. Although there is a wide range in current densities, most devices have J of 3–300 A cm^{-2} at 1 V. The device-to-device

[2] See footnote 1.

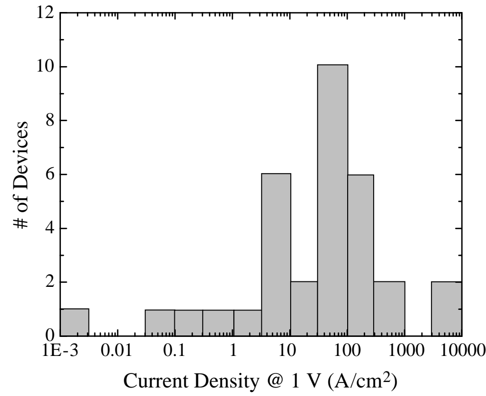

Fig. 5. A histogram plot for observed current densities of all the working molecular devices.

variation can be attributed to fluctuations in the actual device size, formation of partial multilayer (Table 1), or difference in contact geometry introduced during fabrication. The detailed metal–molecule contact configuration has been reported to play an important role in the conductance of the metal/molecular junction [24].

Most $I(V)$ characteristics showed asymmetric behavior with current at positive bias being larger than that at negative bias (as shown in Fig. 4(b)). The origin of the asymmetry can be attributed to the asymmetric nature of the two contacts [25]. For example, the average value of the asymmetric ratio, $R = (I \text{ at } 1\text{ V})/(I \text{ at } -1\text{ V})$, was found as ~2.7 and ~24.9 for two different fabrications, which also indicates that there is a variation in fabrication runs. Molecular devices have been observed to degrade in time [21]. In our case, typically current densities decreased over a time period of a month while $I(V)$ shapes remained similar.

3.2. Schottky barrier model vs. tunneling model

One tends to use a Schottky barrier model to explain $I(V)$ of metal/molecule/semiconductor junctions, however a simple tunneling model (the case for metal/insulator/metal junctions) cannot be ruled out, especially when a highly doped semiconductor is used as the substrate as in our case. The Schottky barrier model and tunneling model exhibit distinct temperature dependencies of their transport characteristics, as expressed in Eqs. (1) [26] and (2) [23, 27], respectively:

$$J = A^* T^2 T_N \exp\left(\frac{-q(\Phi_S + \beta V)}{kT}\right)\left\{\exp\left(\frac{qV}{kT}\right) - 1\right\} \tag{1}$$

where A^* is the Richardson constant, k is Boltzmann's constant, T is temperature, Φ_S is the Schottky barrier height, V is the applied bias, $n = 1/(1-\beta)$ is the ideality factor, and T_N is the transmission probability for tunneling through the molecular layer. Current

Table 2
Summary of $I(V, T)$ measurement results

Device	Size (μm)	J (A cm^{-2} at 1 V)	Temperature dependence	Thermal activation barrier (meV)
#1	5×5	10^{-3}	No	
#2	10×10	0.1	Weak	15
#3	25×25	10	Weak	10

It is noted that there is no scaling correlation of current densities with device size.

density from the tunneling model is expressed as [23, 27]

$$J = \left(\frac{e}{4\pi^2 \hbar d^2}\right) \left\{ \left(\Phi_T - \frac{eV}{2}\right) \exp\left[-\frac{2\sqrt{2m}}{\hbar}\alpha\sqrt{\Phi_T - \frac{eV}{2}}d\right] - \left(\Phi_T + \frac{eV}{2}\right) \exp\left[-\frac{2\sqrt{2m}}{\hbar}\alpha\sqrt{\Phi_T + \frac{eV}{2}}d\right]\right\} \quad (2)$$

where m is the electron mass, h $(=2\pi\hbar)$ is Planck's constant, d is the tunneling barrier width, Φ_T is the tunneling barrier height, and α is a unitless adjustable parameter that is introduced to modify the simple rectangular barrier model or to account for an effective mass ($m^* = \alpha^2 m$) [23]. The device structures that can be explained by the Schottky barrier model (Eq. (1)) will have significant temperature dependence in their $I(V)$ characteristics [26, 28], while devices that follow the tunneling model have no dependence on temperature.

In order to determine the conduction mechanism, we performed $I(V, T)$ measurements on three molecular devices that were chosen randomly and have different current densities. The $I(V, T)$ results are summarized in Table 2 with their current densities and temperature-dependencies. The measured $I(V, T)$ data and the corresponding Arrhenius plot are shown in Fig. 6 for device #3 (from Table 2). We observed no or little temperature dependence for all devices, indicating that the main conduction mechanism is tunneling. Device #1 showed no temperature dependence in $I(V)$s measured from 300 to 10 K, while devices #2 and #3 (measured from 300 to 100 K) showed little temperature dependence with a weak thermal activation. The thermal activation barrier height Φ_{TH} (from $I \propto \exp(-\Phi_{TH}/kT)$) was determined as $\sim$15 and $\sim$10 meV for devices #2 and #3, respectively. Compared with such weak thermal barriers, thermionic Schottky barrier height for molecule/semiconductor systems has been reported as larger than 500 meV [10].

Schottky barrier type conduction is expected when a lightly doped semiconductor material is used as the substrate; here, tunneling is the dominant transport mechanism since a highly doped n-Si substrate is used in our study. The electron conduction is expected to be tunneling when the Fermi levels of contacts lie within the HOMO–LUMO gap (HOMO: highest occupied molecular orbital, LUMO: lowest unoccupied molecular orbital) of a short-length organic molecule [29]. The metal/TMS-EP/Si structure studied in our case is similar to the metal/insulator/metal structure, hence tunneling is expected to be the dominant conduction mechanism. Since XPS data (Fig. 3) indicates that the

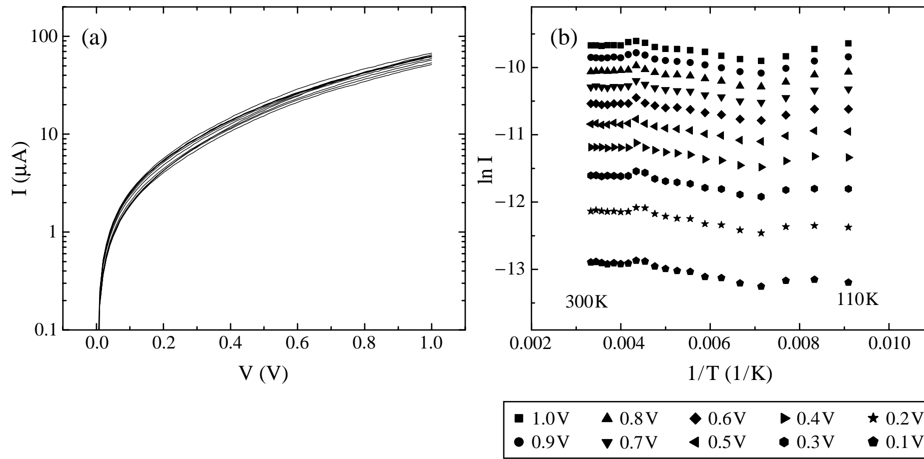

Fig. 6. (a) $I(V,T)$ measurement result for device #3 (Table 2). $I(V)$ data at temperatures from 300 to 110 K with 10 K steps are plotted on a log scale. (b) Arrhenius plot generated from the $I(V)$ data in (a) showing little temperature dependence with a weak thermal activation.

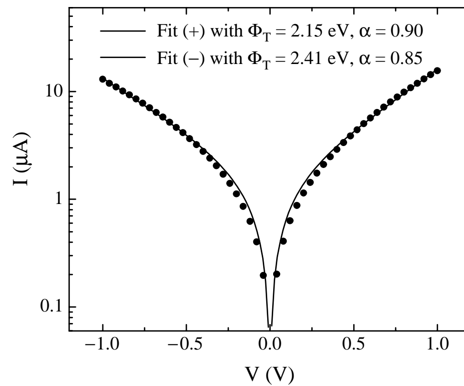

Fig. 7. Measured $I(V)$ data (circular symbols) is compared with calculated one (solid curve) using tunneling model with the optimum fitting parameters of $\Phi_T = 2.15$ eV and $\alpha = 0.90$ (corresponding to $m^* = 0.81$ m) for positive bias region (Fit (+)) and $\Phi_T = 2.41$ eV and $\alpha = 0.85$ (corresponding to $m^* = 0.72$ m) for negative bias region (Fit (−)). Current is plotted on log scale.

molecule/Si interface is free of silicon oxide, the tunneling result obtained from $I(V,T)$ characterizations is due to the TMS-EP molecular structure. This also indicates that there are few defects in our molecular layers, otherwise significant temperature-dependent defect-mediated transport behavior would occur.

The measured $I(V)$ data is fitted with the tunneling model and a representative fitting result is shown in Fig. 7 for a device having $J \sim 3$ A cm^{-2} at 1 V. Sixteen Å (obtained from

Table 1) was used as the tunneling gap width for this fitting. For this device, from nonlinear least squares fitting using (2), the optimum fitting parameters were found as $\Phi_T = 2.15$ eV and $\alpha = 0.90$ (corresponding to $m^* = 0.81$ m) for the positive bias region (Fit (+)) and $\Phi_T = 2.41$ eV and $\alpha = 0.85$ (corresponding to $m^* = 0.72$ m) for the negative bias region (Fit (−)). It is noted that the Φ_T and α values obtained from the tunneling fittings for TMS-EP are not unique due to the device-to-device variations in current densities, which result from the variation of the TMS-EP layer thickness (Table 1) or variation of surface roughness between samples (typical RMS roughness of a 1 μm × 1 μm surface was found as ∼0.2 nm from AFM study).

4. Conclusions

In conclusion, we have fabricated metal/molecule/Si junctions by directly assembling covalently bound molecules (TMS-EP) onto the highly doped n-type Si(111) surface. Current–voltage measurements on these junctions showed nonlinear electrical characteristics with suppressed current densities, as compared with ohmic behavior observed in the control samples (without molecules). The results of temperature-dependent current–voltage measurements indicate that the dominant conduction mechanism is tunneling, rather than Schottky barrier type conduction.

Acknowledgements

We thank James F. Klemic, Ilona Kretzschmar, and Zhijiong Luo for discussions. This work was supported by DARPA/ONR (N00014-01-1-0657), ARO (DAAD19-01-1-0592), AFOSR (17496200110358), NSF (DMR-0095215), NASA (NCC 2-1363), and National Institute of Standards and Technology (60NANB1D0085).

References

[1] A. Aviram, M.A. Ratner (Eds.), Molecular Electronics: Science and Technology, The Annals of the New York Academy of Sciences, vol. 852, The New York Academy of Sciences, New York, 1998.
[2] R.M. Metzger, B. Chen, U. Ho1pfner, M.V. Lakshmikantham, D. Vuillaume, T. Kawai, X. Wu, H. Tachibana, T.V. Hughes, H. Sakurai, J.W. Baldwin, C. Hosch, M.P. Cava, L. Brehmer, G.J. Ashwell, J. Am. Chem. Soc. 119 (1997) 10455.
[3] M.A. Reed, C. Zhou, C.J. Muller, T.P. Burgin, J.M. Tour, Science 278 (1997) 252.
[4] J. Chen, M.A. Reed, A.M. Rawlett, J.M. Tour, Science 286 (1999) 1550.
[5] C.P. Collier, G. Mattersteig, E.W. Wong, Y. Luo, K. Beverly, J. Sampaio, F.M. Raymo, J.F. Stoddart, J.R. Heath, Science 289 (2000) 1172.
[6] J. Park, A.N. Pasupathy, J.I. Goldsmith, C. Chang, Y. Yaish, J.R. Petta, M. Rinkoski, J.P. Sethna, H.D. Abruna, P.L. McEuen, D.C. Ralph, Nature 417 (2002) 722.
[7] A. Ulman, An Introduction to Ultrathin Organic Films from Langmuir–Blodgett to Self-Assembly, Academic Press, Boston, 1991.
[8] J.M. Buriak, Chem. Rev. 102 (2002) 1271.
[9] C. Boulas, J.V. Davidovits, F. Rondelez, D. Vuillaume, Phys. Rev. Lett. 76 (1996) 4797.
[10] Y. Selzer, A. Salomon, D. Cahen, J. Chem. Phys. B 106 (2002) 10432.
[11] D. Li, A. Bishop, Y. Gim, X.B. Shi, M.R. Fitzsimmons, Q.X. Jia, Appl. Phys. Lett. 73 (1998) 2645.
[12] A. Vilan, A. Shanzer, D. Cahen, Nature 404 (2000) 166.

[13] I.H. Campbell, S. Rubin, T.A. Zawodzinski, J.D. Kress, R.L. Martin, D.L. Smith, Phys. Rev. B 54 (1996) 14321.
[14] M. Delamar, R. Hitmi, J. Pinson, J.M. Saveant, J. Am. Chem. Soc. 114 (1992) 5883.
[15] P. Allongue, C.H. de Villeneuve, J. Pinson, F. Ozanam, J.-N. Chazalviel, X. Wallart, Electrochim. Acta. 43 (1998) 2791.
[16] P. Allongue, M. Delamar, B. Desbat, O. Fagebaume, R. Hitmi, J. Pinson, J.-M. Saveant, J. Am. Chem. Soc. 119 (1997) 201.
[17] D.V. Kosynkin, J.M. Tour, Org. Lett. 3 (2000) 993.
[18] M.P. Stewart, F. Maya, D.V. Kosynkin, S.M. Dirk, J.J. Stapleton, C.L. McGuiness, D.L. Allara, J.M. Tour, submitted for publication.
[19] P. Hartig, J. Rappich, Th. Dittrich, Appl. Phys. Lett. 80 (2002) 67.
[20] NIST X-ray photoelectron spectroscopy database version 3.2. Available from http://srdata.nist.gov/xps/.
[21] J.-O. Lee, G. Lientschnig, F. Wiertz, M. Struijk, R.A.J. Janssen, R. Egberink, D.N. Reinhoudt, P. Hadley, C. Dekker, Nano Lett. 3 (2003) 113.
[22] C.R. Kagan, A. Afzali, R. Martel, L.M. Gignac, P.M. Solomon, A.G. Schrott, B. Ek, Nano Lett. 3 (2003) 119.
[23] W. Wang, T. Lee, M.A. Reed, Phys. Rev. B 68 (2003) 035416.
[24] M. Di Ventra, S.T. Pantelides, N.D. Lang, Phys. Rev. Lett. 84 (2000) 979.
[25] S. Datta, W. Tian, S. Hong, R. Reifenberger, J.I. Henderson, C.P. Kubiak, Phys. Rev. Lett. 79 (1997) 2530.
[26] E.A. Rhoderick, R.H. Williams, Metal–Semiconductor Contacts, Clarendon Press, Oxford, UK, 1988.
[27] J.G. Simmons, J. Appl. Phys. 34 (1963) 1793.
[28] S.M. Sze, Physics of Semiconductor Devices, Wiley, New York, 1981.
[29] M.A. Ratner, B. Davis, M. Kemp, V. Mujica, A. Roitberg, S. Yaliraki, in: A. Aviram, M. Ratner (Eds.), Molecular Electronics: Science and Technology, The Annals of the New York Academy of Sciences, vol. 852, The New York Academy of Sciences, New York, 1998.